The back-analysis of shear modulus reduction with strain in weathered mudstone beneath an instrumented embankment

Kevin BRIGGS[1], Yuderka TRINIDAD GONZÀLEZ[2], Gerrit MEIJER[3], William POWRIE[1], Simon BUTLER[4], Nick SARTAIN[5]

[1]University of Southampton, Southampton, United Kingdom
[2]Iowa State University, Ames, IA, United States
[3]University of Bath, Bath, United Kingdom
[4]HS2 Ltd, seconded from AtkinsRéalis, Birmingham, United Kingdom
[5]Arup, Birmingham, United Kingdom

Corresponding author: Kevin Briggs (K.Briggs@soton.ac.uk)

Abstract

Full-scale earthworks trials were undertaken in advance of the construction of the High Speed 2 (HS2) railway between London and the West Midlands. They provided in-situ measurements of the ground response due to loading and unloading from the overlying earthworks. Results from the trials were used by HS2 Ltd to refine the design parameters, make cost savings and eliminate the need for engineering interventions to control ground movement. However, the instrumented trials also provided more fundamental information about the engineering properties of the ground. This is particularly useful in difficult ground such as weathered mudstone.

This paper presents results from back-analyses of in-situ measurements at an embankment trial, 14 km north of Banbury, to measure the stiffness of the underlying, weathered mudstone.

Geophysical shear wave velocity measurements were undertaken to determine the in-situ shear modulus at very small strain. These showed that the shear modulus of the ground profile increased linearly with depth in the clay, consistent with empirical equations. During well-defined construction loading stages, measurements were obtained from extensometers installed beneath the embankment. These were used to measure deformation and strains within the underlying ground profile and calculate the in-situ shear modulus. The shear modulus was normalised to compare with empirical equations for shear modulus reduction with strain. The results showed that the gradient of the normalised, non-linear stiffness of the clays was comparable with those measured in laboratory tests of fine-grained soils, at a range of strains. However, the values for the reference strain (where the maximum shear modulus reduces by 50%) were lower than was predicted by the empirical equations.

Keywords: Instrumentation, Monitoring, Mudstone, Stiffness

1. Introduction

The stiffness of stiff clays and weak rocks reduces rapidly with strain over the medium strain range of 0.001% to 0.1% and is highly non-linear (Jardine et al 1984; Atkinson 2000; Clayton 2011; O'Brien et al 2023). This corresponds to typical strain levels around geotechnical structures (Clayton 2011) and is therefore an important consideration for design (O'Brien et al 2023). Small-strain stiffness can be measured using in-situ geophysical tests and in the laboratory using bender elements or resonant column apparatus. Stiffness at larger strains can be obtained from conventional and advanced triaxial testing of laboratory samples. It is also possible to measure stiffness over a range of strain levels from the back-analyses of structural behaviour at full-scale (Burland 1989; Ng et al 1998). This is particularly appropriate for embankment construction, where movement is predominately one-directional (i.e. vertical) and vertical stress changes in the ground are relatively insensitive to nonlinear stress-strain behaviour, stiffness anisotropy and increasing stiffness with depth (Burland et al 1978).

The construction of the HS2 railway between London and the West Midlands provided an opportunity to obtain monitoring data from earthworks founded on a range of stiff clays and weak rocks in central England, including those from the Cretaceous, Jurassic and Triassic periods. This paper describes the use of field instrumentation to measure the in-situ shear moduli of stiff fissured clays and weathered mudstones of the Charmouth Mudstone Formation (Lias Group). Surface loading, pore water pressures and ground deformations were measured during the construction of an instrumented trial embankment. These were compared with site investigation data and in-situ geophysical measurements.

2. The trial embankment

The trial embankment was located north of Banbury (52°11'17"N, 1°20'25"W) in Oxfordshire (Figure 1). It was constructed in stages between 7 November 2020 and 9 December 2020 to form an embankment 150 m long and 95 m wide (at the base), with a slope angle of 23°. The embankment was measured by aerial drone surveys during construction and reached a final height of 8.2 m. It was constructed using fill from a cutting excavation located directly to the south. The fill material and the ground beneath the embankment consisted of clays and mudstones of the Charmouth Mudstone Formation (Lias Group). Borehole excavations beneath the embankment footprint showed (i) weathered, firm to locally stiff fissured clay to 5 mbgl, (ii) weathered, stiff and very stiff fissured clay to 12-13 mbgl and (iii) weathered and unweathered, fissured mudstone below. A band of calcareous siltstone (i.e. limestone) was observed between 18 and 20 mbgl.

Instruments were installed beneath the centre of the embankment and beneath the southeastern edge of the crest of the embankment in advance of construction (Figure 1). They included total pressure cells (PC1 & PC2) to measure the load from the embankment, piezometers (PIEZO1 & PIEZO2) to measure pore water pressure and in-line extensometers (EXT1 & EXT2) to measure the vertical displacement of the ground profile. The instruments were installed between August and October 2020 and were logged at hourly intervals from 5 November 2020 until the end of construction on 9 December 2020. The piezometer measurements showed that pore water pressures rapidly increased in response to embankment construction, with limited drainage (1-2 kPa reduction) between the construction stages (Briggs et al 2024).

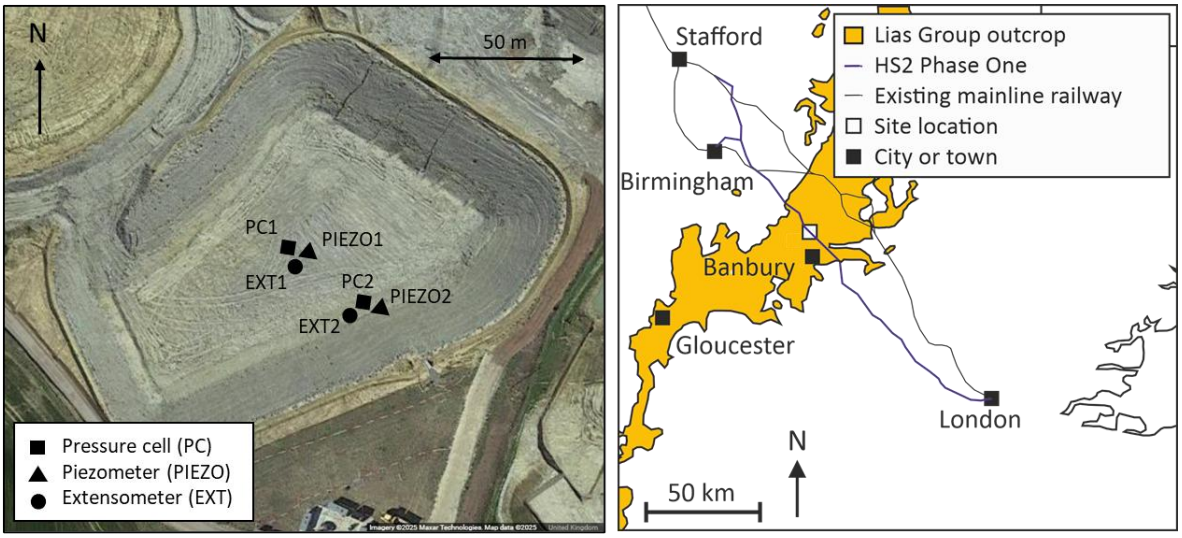

(a) (b)

Figure 1: (a) The trial embankment and instrument locations. (b) The site is located in a Lias Group outcrop north of Banbury (52°11'17"N, 1°20'25"W) in Oxfordshire. Map data: Google, Maxar Technologies.

2.1 Total pressure cells

Total pressure cells (RST Instruments, LPTPC09-V-LP) were installed and calibrated in shallow pits beneath the trial embankment prior to construction (Figure 1). Briggs et al (2025) used the pressure cell measurements and the known embankment height from three drone surveys to estimate the unit weight of the embankment fill (≈22 kN/m^3). The pressure cell measurements were used to estimate the change in embankment height with time (Figure 2) beneath the centre of the embankment (PC1) and beneath the edge of the embankment crest (PC2). The results in Figure 2 were used to select the embankment height at eight loading stages (i.e. embankment construction stages) for use in the stiffness analyses.

2.2 Extensometers

Vibrating wire in-line extensometers (RST Instruments EXINLINE-1100) were installed beneath the centre of the embankment (EXT1) and beneath the edge of the embankment crest (EXT2), to 60 mbgl and 50 mbgl respectively. Each extensometer included six Borros hydraulic anchors, connected to six displacement transducers in series, separated by stainless steel rods within a PVC sheath. The anchors were hydraulically activated in ascending order from the base of the borehole and grouted in place. The displacement of the

anchors increased with each embankment loading stage, with the greatest displacements in anchors near the ground surface. There was minimal (<1 mm) displacement of the anchors located below 25 to 30 mbgl.

Figure 3 shows the displacement (δ_{Layer}) between adjacent extensometer anchors at EXT1, beneath the centre of the embankment. The measurements for the anchors between 0 mbgl and 5 mbgl were an order of magnitude greater than those shown in Figure 3 and have therefore been omitted for clarity. Figure 3 shows that the distance between the pairs of adjacent anchors reduced (i.e. reducing layer thickness) as the embankment loading increased.

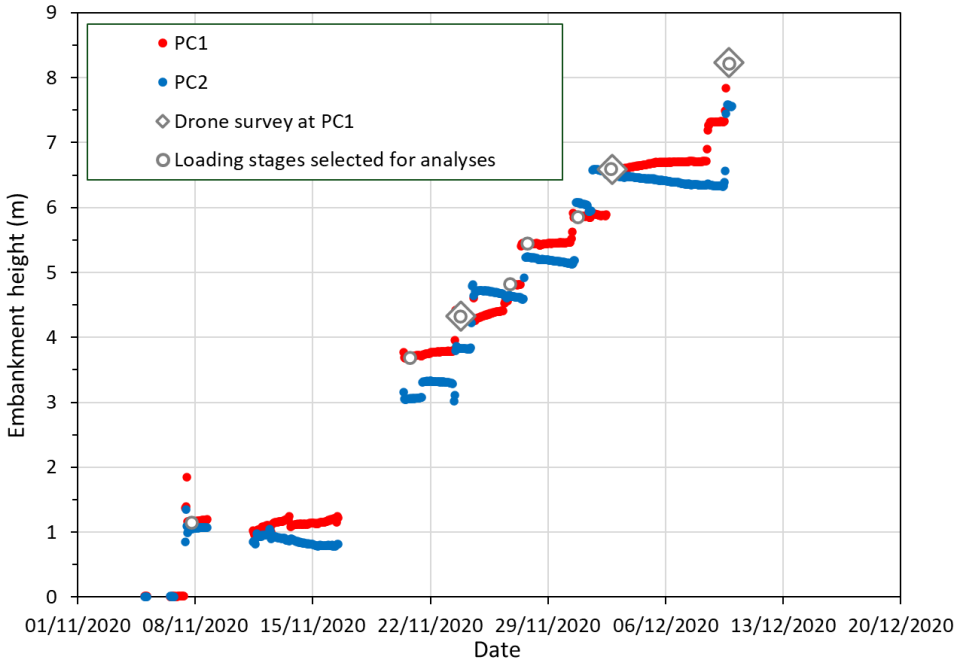

Figure 2: The change in embankment height during construction, back calculated from pressure cell measurements (PC1 & PC2) and calibrated with drone survey measurements (Adapted from Briggs et al 2025)

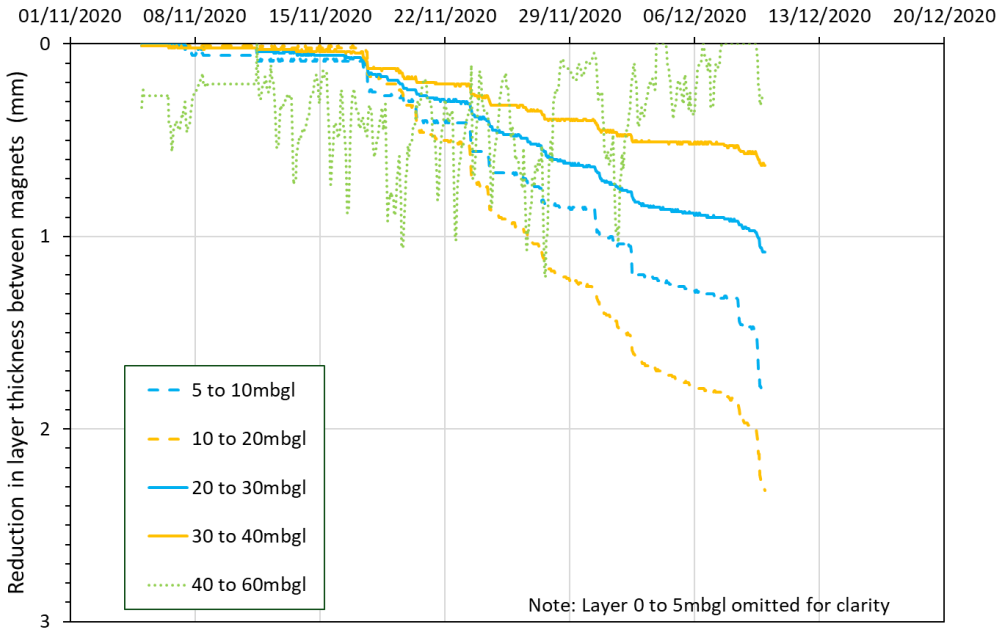

Figure 3: The reduction in layer thickness between extensometer anchors installed beneath the centre of the trial embankment at EXT1. Note that the extensometer anchors are not equally spaced (From Briggs et al 2025).

2.3 In-situ testing

Downhole seismic tests were undertaken by a specialist contractor in four boreholes (DHGEO 2, 3, 6 & 7) located approximately 250 m to the south of the trial embankment. S-waves were generated by striking the end of a timber sleeper and were detected by a BGK-7 multi-element geophone. Briggs et al (2025) used the S-wave velocities and unit weight measurements to produce a profile of shear modulus at very small strain (G_0) with depth. This was considered to be the maximum shear modulus (G_{max}). For comparison, a profile of maximum shear modulus with depth was determined using the Vardanega & Bolton (2013) empirical correlation for fine-grained soils tested in laboratory conditions:

$$\frac{G_{max}}{p'_r} = \frac{B}{v^{2.4}}\left(\frac{p'}{p'_r}\right)^{0.5}$$

where p' is the mean effective stress, p'_r is a reference stress (taken as 1 kPa) and v is the specific volume of eighteen triaxial samples obtained near the trial embankment (Briggs et al 2025). A soil structure coefficient, B, was selected for a typical fine-grained soil (B = 20,000) and for an overconsolidated aged clay (B = 50,000).

Figure 4 shows the profile of maximum shear modulus with depth from the interpretation of the downhole seismic tests and from the Vardanega & Bolton (2013) equation. It shows a bi-linear increase in G_{max} with depth. The measurements in the weathered clay to 8 mbgl agree with the Vardanega & Bolton profile for typical fine-grained soils (i.e. B = 20,000). In the less-weathered clay and mudstone below 8 mbgl (from 9 to 20 mbgl) the measurements show greater values of G_{max}. They compare with the Vardanega & Bolton profile for overconsolidated aged clay (i.e. B = 50,000).

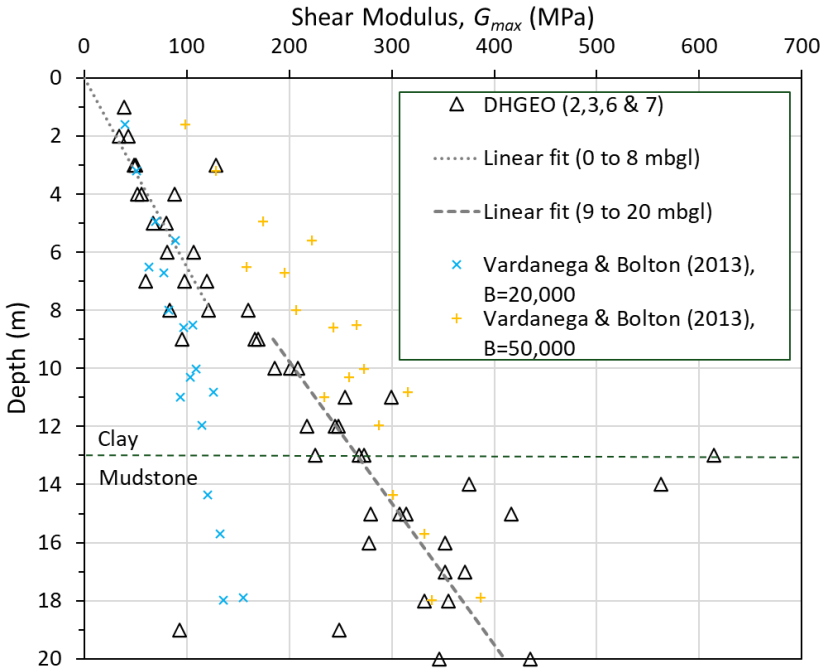

Figure 4: The maximum shear modulus (G_{max}) derived from downhole seismic tests. These are compared to the Vardanega & Bolton (2013) model for typical fine-grained soils (B = 20,000) and overconsolidated aged clay (B = 50,000), using the specific volume of triaxial samples from the site. Adapted from Briggs et al (2025).

3. Method

The embankment loading (Figure 2) and extensometer (Figure 3) measurements were used to calculate the in-situ shear modulus ($G_{Layer,Stage}$) of the clay and mudstone layers beneath the embankment at chosen stages of embankment construction. These were normalised by G_{max} values obtained from downhole seismic tests (Figure 4), for comparison with shear modulus reduction with strain curves for different plasticity indices (Vardanega & Bolton 2013). The analyses assumed an immediate, undrained ground response to surface loading. The method included the following steps:

Step 1: Construction of the embankment increased the total stresses (σ_z, σ_x and τ_{zx}) in the underlying ground. These were calculated for each layer (i.e. between adjacent extensometer anchors) beneath the embankment

at selected stages of construction (Figure 2). The changes in stress were calculated using the analytical equations for stress increments in a plane-strain elastic half-space beneath a surface load, summarised by Poulos & Davis (1974). Changes in stress were calculated at the top ($\Delta\sigma_{Top}$), midpoint ($\Delta\sigma_{Mid}$) and base ($\Delta\sigma_{Base}$) of the layers beneath the centre of the embankment (EXT1) and beneath the edge of the embankment crest (EXT2). These were used to derive the weighted average change in stress in each layer at each loading stage ($\Delta\sigma_{zLayerAve,Stage}$, $\Delta\sigma_{xLayerAve,Stage}$, $\Delta\tau_{LayerAve,Stage}$) using Simpson's rule (Atkinson 1989).

Step 2: The average vertical strain of each layer was calculated for each construction stage ($\varepsilon_{zLayer,Stage}$) from the relative displacement between the extensometer anchors ($\delta_{zLayer,Stage}$), relative to their initial spacing (Z_{0Layer}):

$$\varepsilon_{zLayer,Stage} = \frac{\delta_{zLayer,Stage}}{Z_{0Layer}}$$

Vertical strains were calculated for three layers beneath the centre of the embankment at EXT1 (0 to 5 mbgl, 5 to 10 mbgl and 10 to 20 mbgl) and three layers beneath the edge of the embankment crest at EXT2 (0 to 2.5 mbgl, 2.5 to 7.5 mbgl and 7.5 to 15 mbgl).

Step 3: The operational secant shear modulus was calculated for each layer and embankment loading stage ($G_{Layer,Stage}$) using an isotropic, linear elastic stress-strain relationship (Equation 1.36c in Poulos & Davis 1974):

$$G_{Layer,Stage} = \frac{1}{2\varepsilon_{zLayer,Stage}}\left[(\Delta\sigma_{zLayerAve,Stage}(1-\upsilon_u)) - (\upsilon_u\Delta\sigma_{xLayerAve,Stage})\right]$$

where v_u is the undrained Poisson's ratio (taken as 0.5).

Step 4: The plane-strain shear stress invariants were calculated to find the maximum shear stress ($\Delta\tau_{Layer\ Ave,Stage}$), for comparison with the Vardanega & Bolton (2013) laboratory test results using:

$$\Delta\tau_{Layer\ Ave,Stage} = \sqrt{\frac{1}{4}\left(\Delta\sigma_{zLayer\ Ave,Stage} - \Delta\sigma_{xLayer\ Ave,Stage}\right)^2 + \Delta\tau^2{}_{xzLayer\ Ave,Stage}}$$

The operational secant shear modulus ($G_{Layer,Stage}$) and maximum shear stress ($\Delta\tau_{Layer\ Ave,Stage}$) were used to calculate the in-situ, plane-strain shear strain invariant ($\gamma_{Layer,Stage}$):

$$\gamma_{Layer,Stage} = \frac{\Delta\tau_{LayerAve,Stage}}{G_{Layer,Stage}}$$

Step 5: Finally, the secant shear modulus for each layer and embankment loading stage ($G_{Layer,Stage}$) was normalised by the maximum shear modulus (G_{max}) at the midpoint of each layer. Values of G_{max} were derived from the linear regression fits shown in Figure 4.

Step 6: Normalised secant shear modulus reduction with strain curves were calculated for a range of plasticity indices using the Vardanega & Bolton (2013) empirical relationship for fine-grained soils:

$$\frac{G}{G_{max}} = \frac{1}{1+\left(\frac{\gamma}{\gamma_{ref}}\right)^{\alpha}}$$

and

$$\gamma_{ref} = J\left(\frac{I_p}{1000}\right)$$

where γ is the shear strain, γ_{ref} is the reference shear strain at $G = 0.5G_{max}$, α is a fitting parameter (set equal to 0.736, as used in Vardanega & Bolton (2013)), I_p is the plasticity index (expressed as a fraction rather than a percentage) and J is a regression coefficient relating I_p and γ_{ref} (where J = 2.2 in Vardanega & Bolton (2013)).

4. Results

Figure 5a shows the normalised secant shear modulus and shear strain of the six layers beneath the embankment, for eight loading stages. The results show decreasing normalised secant shear modulus (G/G_{max}) with increasing shear strain. Most of the results from the shallowest layers (0 to 5 mbgl) are close to the Vardanega & Bolton (2013) model for a plasticity index (I_p) of 5%. The results from the layer between 2.5 and

7.5 mbgl are close to the Vardanega & Bolton (2013) model for a plasticity index (I_p) of 15%. This layer consists of weathered, stiff and very stiff fissured clay with a plasticity index (I_p) of ≈31% (Briggs et al. 2025). The results from the less-weathered clays and weathered mudstones at greater depth (5 to 20 mbgl and I_p ≈24-28%) are aligned with the Vardanega & Bolton (2013) model for a plasticity index (I_p) of 5%. The results from the trial embankment align with the reduction trend of the Vardanega & Bolton (2013) model, as determined by parameter α, but show lower values of the reference strain (γ_{ref}).

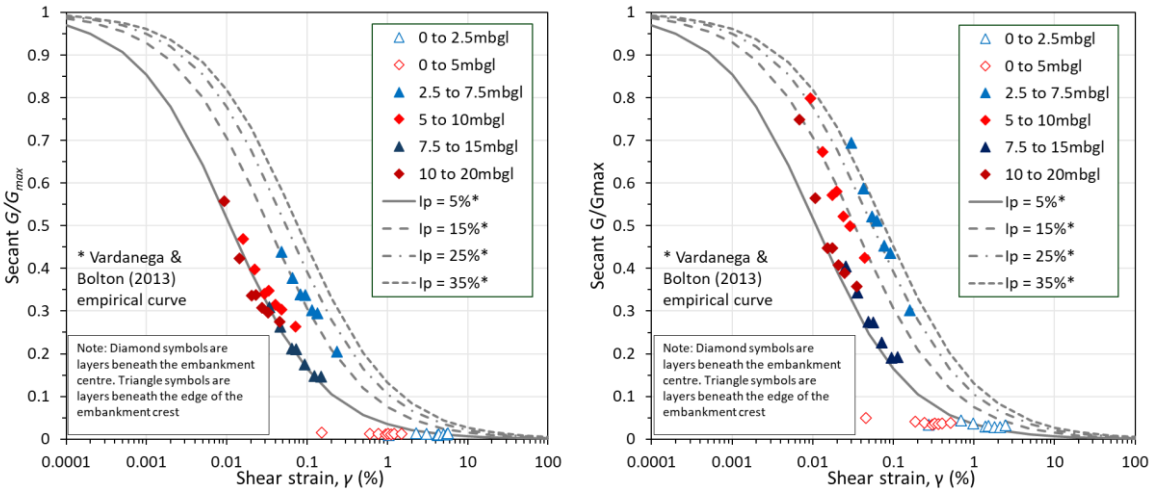

Figure 5: (a) Calculated normalised secant shear modulus with strain for layers beneath the trial embankment, compared with results from the Vardanega & Bolton (2013) model for soils with plasticity indices of 5% to 35%. (b) The results assuming a reduced undrained Poisson's ratio (ν_u = 0.458). Note that the approximate plasticity indices of the soil layers were 33% (0 to 2.5 mbgl), 31% (2.5 to 7.5 mbgl) and 26% (7.5 to 15 mbgl).

The results in Figure 5a assume undrained conditions with no volume change (i.e. ν_u = 0.5), but some undrained volume change may have occurred due to the compressibility of the water or dissolved air in the stiff clay and mudstone (Briggs et al. 2024). Briggs et al (2025) explored the influence of assuming a reduced undrained Poisson's ratio (ν_u = 0.458) to account for measurements of Skempton's (1954) B value of less than unity at the trial embankment (Briggs et al 2024). This produced results (Figure 5b) for the intermediate layers (2.5 to 7.5 mbgl and 5 to 10 mbgl) with higher values of reference strain (i.e. increased G/G_{max} and decreased γ). These aligned more closely with the Vardanega & Bolton (2013) model for I_p ≈ 15-25%, which is lower than the in-situ plasticity index of these layers (I_p ≈ 28-31%).

5. Conclusions

Extensometers installed beneath a trial embankment and nearby downhole geophysical measurements were used to calculate (i) the maximum shear modulus (G_{max}) and (ii) the reduction of normalised secant shear modulus (G/G_{max}) with strain in weathered mudstone beneath an embankment. Extensometer anchors installed at multiple depths allowed the shear modulus of the ground to be calculated for a range of strains that are relevant for the serviceability design of geotechnical structures (<1% strain). This demonstrates the use of field instrumentation to measure the stiffness of the ground profile, in addition to its more routine use for monitoring ground deformation during construction. From this, the following conclusions can be drawn about the stiffness of weathered mudstones and their response to embankment loading:

1. The maximum shear modulus (G_{max}) of the ground beneath the trial embankment increases with depth and is influenced by the in-situ weathering profile. The more weathered, stiff and very stiff fissured clays extend to 8 mbgl and their G_{max} profile can be characterised by the Vardanega & Bolton (2013) empirical correlation for a typical fine-grained soil (i.e. B = 20,000). Below this depth, the ground profile transitions from weathered clay to weathered mudstone and can be characterised below 11 mbgl by the Vardanega & Bolton (2013) empirical correlation for overconsolidated, aged clay (i.e. B = 50,000). This transition compares to the gradational weathering profile observed in boreholes at the trial embankment site and the surrounding outcrop of the Charmouth Mudstone Formation (Briggs et al 2025)

2. The analyses show that the Vardanega & Bolton (2013) empirical equation for normalised secant shear modulus reduction with strain compared favourably with the measurements beneath the embankment (from 0 to 20 mbgl). The more-weathered and plastic clays at shallower depth (2.5 to 7.5 mbgl) showed larger values of reference strain (γ_{ref}), the shear strain at which G/G_{max} = 0.5, than the less-weathered clay and mudstone at greater depth (5 to 20 mbgl). The measurements are in general agreement with the Vardanega & Bolton (2013) empirical correlations for varying plasticity index. However, the plasticity indices of the best-fitting Vardanega & Bolton (2013) curves (I_p of 5 - 15%) were much lower than the plasticity indices measured for clays beneath the trial embankment (I_p of 24 - 33%).

3. A simple method for calculating the reduction of normalised secant shear modulus (G/G_{max}) with strain has been demonstrated for a weathered mudstone profile. This requires downhole geophysical measurements of maximum shear modulus, extensometer measurements beneath the loaded area and an estimation of the stress increments at depth. There is an opportunity to undertake similar analyses where extensometers have been installed beneath embankments founded on weathered mudstones or on ground where it may be difficult to obtain undisturbed samples for advanced laboratory testing.

Acknowledgements

This work was supported by the Royal Academy of Engineering and HS2 Ltd under the Senior Research Fellowship scheme (RCSRF1920\10\65) and the ACHILLES Engineering and Physical Sciences Research Council (EPSRC) programme grant led by Newcastle University (EP/R034575/1). Thank you to staff at Geo-Observations Ltd, COWI and EKFB for assistance with accessing data and materials. The data were provided by HS2 Ltd. The data presented in this paper are described in Briggs et al (2025) and are available online via the University of Bath institutional repository (Briggs, 2024), at https://doi.org/10.15125/BATH-01353.

References

Atkinson, K. E. (1989). *An Introduction to Numerical Analysis* (2nd ed.). John Wiley & Sons. ISBN 0-471-50023-2.

Burland, J.B., Broms, B.B. and De Mello, V.F., (1978). Behaviour of foundations and structures. State of the art review. *9th International Conference on SMFE*, 2, 495-546.

Burland, J. B. (1989). Small is beautiful: the stiffness of soils at small strains. Ninth Laurits Bjerrum Lecture. *Canadian Geotechnical Journal*, 26, No. 4, 499-516.

Briggs, K.M., Trinidad González, Y., Meijer, G.J., Ridley, A., Powrie, W., Butler, S. and Sartain, N., (2024). The influence of earthworks construction on porewater pressures in clays and mudstones of the Lias Group. *Quarterly Journal of Engineering Geology and Hydrogeology*, 57(4). https://doi.org/10.1144/qjegh2024-036

Briggs, K., (2024). *Dataset of measurements at an instrumented embankment trial on an outcrop of the Charmouth Mudstone Formation (Lias Group) in central England*. Bath: University of Bath Research Data Archive. https://doi.org/10.15125/BATH-01353

Briggs, K.M., Trinidad González, Y., Meijer, G.J., Powrie, W., Butler, S. and Sartain, N., (2025). In-situ shear modulus reduction with strain in stiff fissured clays and weathered mudstones. *Canadian Geotechnical Journal*. https://doi.org/10.1139/cgj-2023-0702

Clayton, C.R.I., (2011). Stiffness at small strain: research and practice. *Géotechnique*, 61(1), pp.5-37.

Jardine, R.J., Symes, M.J. and Burland, J.B., (1984). The measurement of soil stiffness in the triaxial apparatus. *Géotechnique*, 34(3), pp.323-340.

Ng, C.W., Simpson, B., Lings, M.L. and Nash, D.F., (1998). Numerical analysis of a multipropped excavation in stiff clay. *Canadian Geotechnical Journal*, 35(1), pp.115-130.

O'Brien, A.S., Ho, X. and Tan, R., (2023). Non-linear stiffness characterisation–a practical framework. *Proceedings of the Institution of Civil Engineers-Geotechnical Engineering*, pp.1-15.

Poulos, H.G., & Davis, E.H., (1974). *Elastic solutions for soil and rock mechanics*, John Wiley & Sons New York. ISBN 0-471-69565-3.

Skempton, A.W., (1954). The pore-pressure coefficients A and B. *Geotechnique*, 4(4), pp.143-147.

Vardanega, P.J. and Bolton, M.D., (2013). Stiffness of clays and silts: Normalizing shear modulus and shear strain. *Journal of Geotechnical and Geoenvironmental Engineering*, 139(9), pp.1575-1589.